Bollettino di Geofisica Teorica ed Applicata Vol. 60, n. 4, pp. 645-656; December 2019
DOI 10.4430/bgta0280

Evaluation of gas hydrate structures: results from an experiment in the South China Sea using the marine controlled-source electromagnetic method

L. Wang[1], S. Xiong[2], Y. Li[3] and J. Jing[1]

[1] *School of Geophysics & Information Technology, China University of Geosciences, Beijing, China*

[2] *China Aero Geophysical Survey & Remote Sensing Center for Natural Resources, Beijing, China*

[3] *Beijing Information Science & Technology University, Beijing, China*

(Received: 12 November 2018; accepted: 2 May 2019)

ABSTRACT This paper presents the preliminary results of the application of Marine Controlled-Source Electromagnetic (MCSEM) detection in the South China Sea in 2014. Electromagnetic fields transmitted by a horizontal electric dipole source that was towed in the deep sea were measured by 4 receivers anchored to the seafloor at 600-m intervals. Specialised data processing is critical to the results and improves the signal-to-noise ratio of MCSEM data. Our resistivity results and Natural Gas Hydrate (NGH) saturation results showed three high-resistivity layers beneath the survey line. Integrated with other seismic and well data from the same region, we hypothesise that the first resistivity layer anomaly might have been caused by the accumulation of large amounts of NGH at a depth of 200 m, whereas the second layer, according to the conceptual model, might be due to a considerable volume of NGH near the seafloor.

Key words: marine controlled-source electromagnetic method, electrical resistivity survey, NGH, South China Sea.

1. Introduction

Chave *et al*. (1991) proposed, using Marine Controlled-Source Electromagnetic (MCSEM), measurements for hydrocarbon exploration and for imaging the distributions of potential alternative energy sources (Chave and Thomson, 1987; Max *et al*., 2006; Boudou *et al*., 2008). At that time, seismic methods were routinely used to determine the presence of gas from a Bottom-Simulating Reflector (BSR). However, there have been cases in which gas hydrates exist but are not detected via a BSR (Yuan and Edwards, 2000). Moreover, marine geological terrains with high-amplitude reflections, such as carbonate reefs, volcanic rocks and submarine permafrost, are difficult to image by using seismic data, as their diffuse upper boundaries make interpretation ambiguous.

To avoid the uncertainty caused by the potential absence of a BSR where Natural Gas Hydrate (NGH) exists, researchers use the working hypothesis that rocks with relatively high seismic velocity contrasts also exhibit geophysical properties that are different from those of surrounding

© 2019 – OGS

sediment (Gallardo and Meju, 2004). Logging data, as important supporting evidence (Pearson *et al*., 1986), indicate higher resistivity in zones containing NGH or oil than in normal sediment (Collett and Ladd, 2000; Max, 2003). This application of logging data has led to the development of the MCSEM technique.

Because of the inaccuracy of seismic indicators and the high cost of deep well exploration (Constable, 2010), MCSEM detection, as an alternative method (Constable and Srnka, 2007; Coffin *et al*., 2008), can be used to measure the resistivity in marine environments and map the NGH distribution. This method has been applied in many NGH zones (Yuan and Edwards, 2000; Weitemeyer *et al*., 2006; Constable and Srnka, 2007; Goto *et al*., 2009; Jegen *et al*., 2014), and many papers have reported successful MCSEM surveys in various locations, including offshore Taiwan (Hsu *et al*., 2014), the Gulf of Mexico (Evans, 2007), NEPTUNE Canada (Swidinsky *et al*., 2013), and the West Nile Delta (Swidinsky *et al*., 2015). Many MCSEM seabed logging applications (Boudou *et al*., 2008; Max and Johnson, 2014) have demonstrated that MCSEM can be used as a secondary method in NGH exploration. Furthermore, we can adopt different controlled-source frequencies to reach different exploration depths (Key, 2009). The MCSEM method was also able to accurately define the boundaries of the methane hydrate zone (Wang *et al*., 2014; Chen *et al*., 2015a; Yin *et al*., 2015).

In this paper, we performed an MCSEM survey in the South China Sea, which has been extensively studied via seismic reflection profiles and well log data. Here, we transformed the resistivity results along the MCSEM transect into a saturation profile using Archie's law. Compared with other data from the same region, the results of the transformation clearly revealed upper abnormal resistivity boundaries. Then, we mapped the gas saturation distribution related to the anomalous resistivity. Finally, we created a conceptual model to analyse the three high-resistivity layers along the survey line, which might have been primarily caused by the large NGH accumulation below the sediment. Some important issues related to the survey area, the instruments, the data process, and the original results are also addressed.

2. MCSEM method

According to the phase equilibrium curve (Max, 1990), the NGH state varies as a function of temperature and pressure. When temperature and pressure are within a stable range, free gas and abundant water are the two important factors for the formation of NGH. In the deep sea, we assume that the seafloor is fully saturated with pore water.

Free gas is a crucial factor for the formation of NGH. When free gas migrates through sediment, fills the pore space and combines with pore water to form NGH, it may change the saturation of crystalline sediment. To some extent, sand resistivity is the ease with which electrons migrate through pore space under a voltage. The higher the porosity is, the clearer the migration pathway. Additionally, the more easily electrons can migrate, the lower the resistivity is. Because NGH is resistive, when it forms in pores, it blocks the migration pathway and resistivity increases. As the saturation of NGH increases, the pathway becomes increasingly blocked. This trend may hinder electron migration and cause the resistivity to increase (Keller, 1966).

We can set a rational function for resistivity and the saturation of sediment that contains NGH following Archie's law.

According to Archie's law (Archie, 1942; Winsauer *et al*., 1952), we can calculate saturation using resistivity after we obtain the porosity, cementation index, saturation index and constant coefficient index.

For 100% water-bearing sand:

$$\rho_0 = F\rho_\omega, \quad F = \alpha\phi^{-m} \tag{1}$$

where α is the tortuosity factor, ρ_0 is the resistivity of the surrounding rock with 100% water saturation, ρ_ω is the resistivity of the gas-bearing sand, F is the formation factor, ϕ is the sediment porosity, and m is the cementation factor.

When the sand voids are filled with water:

$$\rho_t = I\,\rho_0 = S_\omega^{-n}\,\rho_0 \tag{2}$$

where ρ_t is the resistivity of the surrounding rock, I is the resistivity index, S_ω is the pore water saturation factor, and n is the saturation coefficient (often equal to m).

Finally, Archie's law can be expressed as follows:

$$\rho_t = \alpha\phi^{-m}\,S_\omega^{-n}\,\rho_\omega \tag{3}$$

where α is the tortuosity fact or and $S_h = (1 - S_\omega)$ is the fractional gas hydrate concentration.

As shown in Archie's law, a change in ρ_t is predominantly due to ρ_ω. Although it is impossible for us to directly measure saturation, we can measure it indirectly via resistivity.

MCSEM data respond to the resistivity used to measure the electrical properties of geologic formations. Therefore, MCSEM data may represent a promising choice for exploring sediment containing NGH, particularly because the resistivity of hydrocarbon reservoir sands can vary by one or two orders of magnitude from the surrounding sediment.

The exploration instruments, including the transmitter and receivers, used in this survey were designed and built by the Key Laboratory of Geo-Detection Ministry of Education at the China University of Geosciences (Beijing).

During exploration, an array of receivers (Chen *et al*., 2015b) was first sunk to the seabed (Fig. 1). Each receiver includes two orthogonal horizontal white Ag-AgCl (silver-silver chloride) electrodes (10 m). The top of the receiver is a floating ball, and the bottom is a block of stone; together, these parts of the receiver control the vertical movements of the receiver in the deep sea.

Next, the electric dipole-dipole transmitter (Wang *et al*., 2015), which is a deep-tow transmitter with a 130-m towing dipole, was towed approximately 30 m above the seabed. There is a heavy weight attached to the end of the dipole to ensure the height. The coaxial cable from the ship supplied power to the deep-sea transmitter so it could communicate with the onboard monitoring system. Since all receivers are far enough from the transmitter during measurement, the transmitter can be considered the electric dipole source (Qi *et al*., 2014).

During towing, the transmitter generates several signals through the dipoles at the end of its tails. The receiver instruments were able to record the three electric field components and the two magnetic field components.

Finally, an acoustic release instrument was used to release the stone, and the receiver was raised to the surface by the floating ball and collected.

Subsequently, the data from the receivers were transformed into a function of the normalised data (from the transmitter and the receiver) and the offset. Then, the inversion data were displayed as a new map to reveal the distribution of the structures in the sediment and the depth (Chave *et al.*, 1991). The locations where the strength of the electric field is abnormal are possible hydrocarbon reservoirs (MacGregor and Sinha, 2000). We used Archie's law to estimate the average gas hydrate saturation using resistivity information.

2.1. Study area

We performed a technical exploration study in the frequency domain of our methodology to map the structure and the layers that contain NGH on 15 May 2014 (see Fig. 1) (Yin *et al.*, 2008; Yu *et al.*, 2014).

Four receivers were laid on the seafloor, and the transmitter was towed near the seafloor along the survey line. We used a horizontal electric dipole and two copper pipes (blue in Fig. 1) to generate EM signals. A real-time onboard monitoring system tracked the transmitter, altimeter, sensors, and temperature in 3D.

The study region, which is at latitude 16°-23° and longitude 108°-120°, is located in the Pearl River Mouth Basin of the South China Sea. The region is at the southern end of the main portion

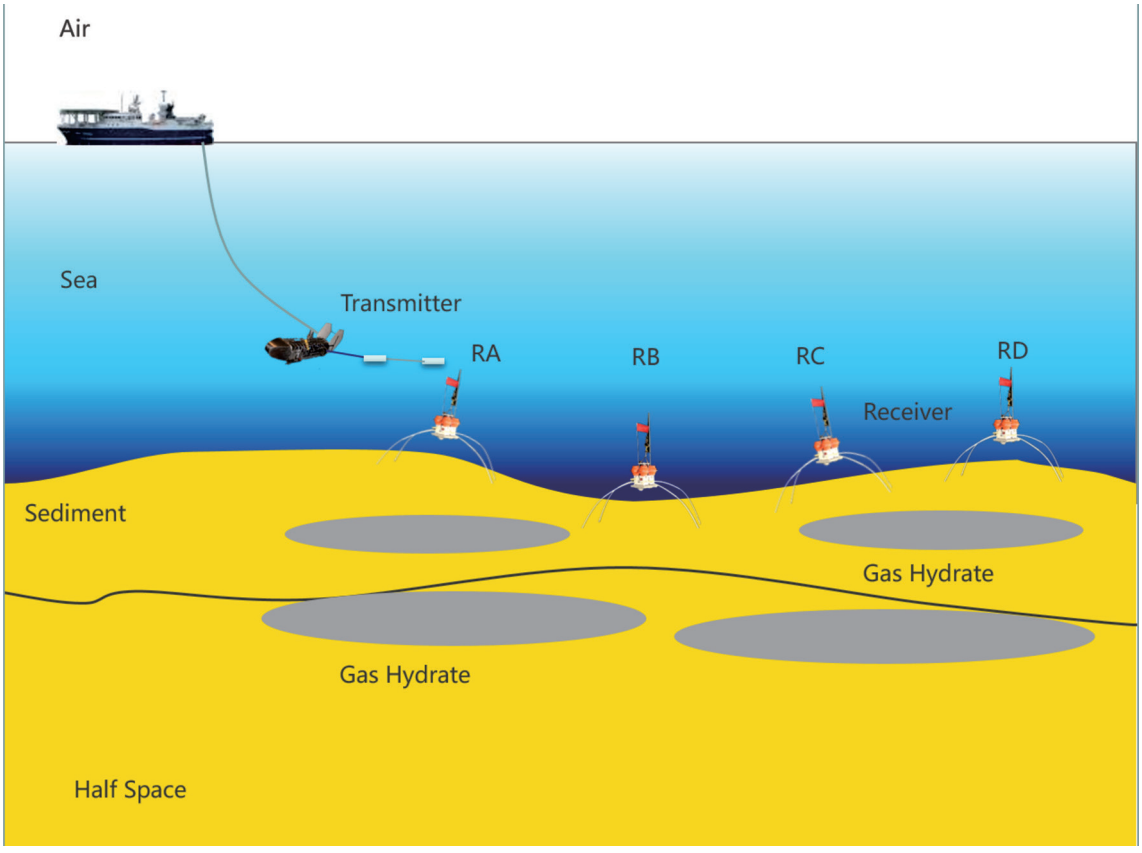

Fig. 1 - Schematic diagram of the MCSEM seabed logging method.

of the South China Sea, west of the Indochina block and east of the Taiwan - Philippine island arc. Convergence occurs between this block and the South Block in southern China (Chen *et al*., 2005). Gas seep sites and chemosynthetic fauna are widespread at the edge of our profile at a depth of 1200 m (Chiu *et al*., 2014). Tectonic activity also affected the area, although the effects were small (Wang *et al*., 2014). Expulsion chimneys, which are upright formations in the survey profile, are well developed and provide a vertical route for free gas migration (Løseth *et al*., 2009; Zhao *et al*., 2015). Fluid in the basin may travel along these routes to locations with appropriate temperatures and pressures for NGH formation (Zhang *et al*., 2000; Sha *et al*., 2005). Furthermore, the landscape is closely associated with the formation of NGH (Liu *et al*., 2010), and the area is located in the Baiyun Sag in a region where NGH has been collected (Shao *et al*., 2001). The seabed is at a depth of 1198 m (see Fig. 2), and the topography of the seafloor includes hills and swells, with a difference of 300 m between the two ends of the survey line.

In our study area, seismic and logging data have been collected previously (Chen *et al*., 2005; Wu *et al*., 2011; Chiu *et al*., 2014), but this study is the first in which the MCSEM method has been used in this survey area. We used two 130-m long copper pipes as electrodes to generate square waveform EM signals. Signal frequencies of 8 Hz, 1 Hz, and 0.5 and 1.5 Hz (a simultaneous double frequency) were used. All signals had a bidirectional amplitude of ±250 A, which was limited by the cable for safety. Four receivers were separated by intervals of 600 m on the seafloor along the profiles.

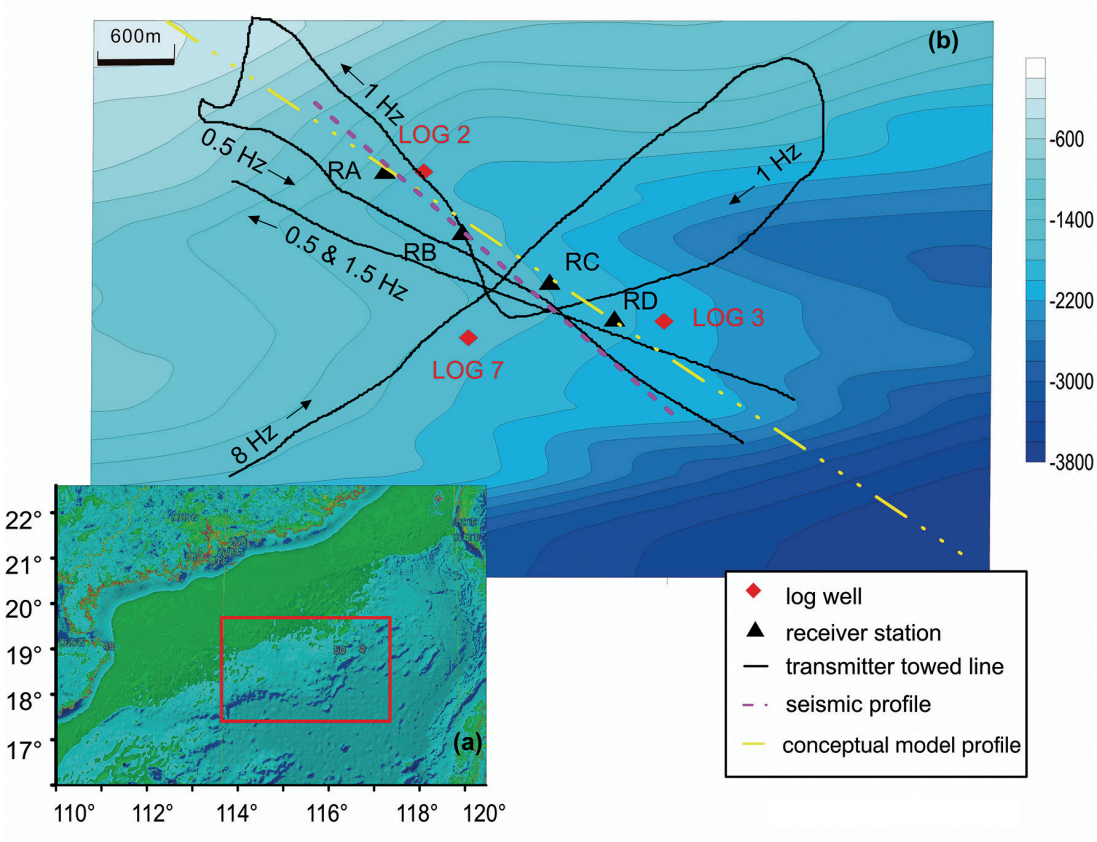

Fig. 2 - Field work location in the South China Sea (a); survey area (b).

The survey consisted of 5 towlines (length: 40 km) and 4 receiver sites (black triangles). The black line represents the towed transmitter line, and the frequency was different at each section. Seismic (pink line) and well log (red diamonds) measurements were concentrated along the same transect.

2.2. Method

The survey lasted 15 days starting on 15 May 2014. First, we installed four receivers on the seabed. Then, we dragged the transmitter for five survey lines with different frequency-domain signals.

During this survey, only three receivers were able to be retrieved; the RB receiver (see Fig. 2) was lost due to a problem with the acoustic release device (Metcalfe *et al*., 2014).

Data processing is important before transforming the original electric and magnetic field data into an interpretable form. The data processing approach was based on several fundamental principles, most of which followed Behrens (2005), which can be summarised as follows.

We classified the three parts of the data set and checked the data quality. For example, for the receiver, we checked the clock drift correction, the antenna length coefficient, the A/D conversion factors, the preamplifier response coefficient of the time series and the frequency spectrum; for the transmitter, we checked the source dipole length, the current coefficient, the waveform spectrum, and the current and frequency stability; for the navigation data, we checked the time error, etc. Then, the data were transformed from the time domain to the frequency domain using the classic fast Fourier transform (FFT) method. During this process, which is called spectral decomposition, time series data were binned, and each bin was tagged with a corresponding timestamp. We choose non-equispaced FFT (NFFT) = 16,384 as the length of the data. The receiver and transmitter spectra were recorded for the same length of time.

Then, we calculated the normalised spectrum (amplitude A and phase ϕ) of the EM field response to the source by dividing the receiver spectrum by the transmitter spectrum:

$$(A,\phi) = A_{R_X} e^{i\phi_{R_X}} / A_{T_X} e^{i\phi_{T_X}} \tag{4}$$

The orientations of the receivers could not be determined using the internal compasses since the receivers fall freely. The receiver orientation is very critical during measurement because partially considering or neglecting receiver orientation may lead to erroneous inversion results (Behrens, 2005; Qi *et al*., 2017). Thus, we have to correct the receiver azimuth using a method such as the polarisation ellipse method (Behrens, 2005; Key, 2011).

Because the direct compass measurement is not the same as the available orientation, we use the polarisation method to find a proper angle (i.e. the horizontal angle with respect to geodetic north). We can subsequently rotate the receiver data to project them, for example, to an inline or crossline direction. Based on the polarisation analysis, the initial azimuth ranges from 0 to 135° and the E field amplification is dispersed from 10^{-7} to 10^{-13} V/m.

The next step is geometric construction. Although three types of data were recorded separately, we choose data in the same time section. Using their timestamps, we merge the navigational data with the processed transmitter-to-receiver EM field data. However, different frequencies have different available offsets; for example, 8 Hz is -600 to 1500 m, 1 Hz is -2000 to 3000 m, and the double frequency (0.5 and 1.5 Hz) is -2700 to 2700 m.

We followed classic subseafloor resistivity models (Constable and Srnka, 2007) for 50 uniform layers at a sea depth from 1198 to 2198 m. Inverting the data to a 1D inversion step keeps the root mean square (RMS) misfit below 1. Based on the azimuth from the polarisation analysis, there was an average RMS normalised data error of 0.89. Fortunately, because we use 1D inversion, we do not have to consider the towline direction. Finally, we generated a profile using the inversion data.

2.3. Results

According to the skin depth law, low-frequency propagation in conductive media is transformed into a distance over which the field strengths are reduced by a factor of 1/e (Weitemeyer, 2008; Weitemeyer *et al*., 2010). The skin depth is:

$$\Delta = \sqrt{\frac{2}{f\mu\rho}} \tag{5}$$

where f is frequency, μ is magnetic permeability, and ρ is resistivity.

There is an inverse proportional relationship between frequencies and detection depths (Key, 2011). Obviously, the 8-Hz signal provides a lower available depth than the 0.5-Hz signal. For a single receiver station, we use the double frequency (0.5 and 1.5 Hz) and include harmonics during the inversion step, followed by multifrequency joint inversion (Key, 2009). The final result contains all the frequencies provided, including the harmonics. While the depth in inversion data is the same, we have to handle the different frequencies. The frequency used and the depth it reaches should be seriously considered. Thus, depth information is constrained during the interpretation step to be below our standard deviation to resolve deep structures (MacGregor and Sinha, 2000).

Fig. 3a shows results of the general resistivity data. According to Archie's law $\rho_t = \alpha\phi^{-m}S_\omega^{-n}\rho_\omega$, in our survey area, we assume that pore water is abundant in the seafloor. Thus, we set $\alpha = 1.0$, $m = 2.2$, $n = 2.0$, $\rho_\omega = 0.3$ Ωm (typically) and $\phi = 50\%$ (on average) (Chen *et al*., 2014; Wang *et al*., 2014; Yu *et al*., 2014). The parameter ϕ may be reduced to 30% near the ridge, and ρ_t is the electrical resistivity, which was derived from the MCSEM data. Then, we obtain the saturation results shown in Fig. 3b.

The seabed is at an approximate depth of 1198 m, the maximum resistivity of the abnormal layer is approximately 3.0 Ωm, and the survey line is from SW to NE. Clearly, there are three abnormal high-resistivity layers. The four receivers at intervals of 600 m are named RA, RB, RC, and RD from left to right in Fig. 3. The RB data were lost; therefore, there are two vague areas, as shown in the rectangular area in Fig. 3. We can see that the first high-resistivity layer is approximately 50 to 100 m below the sea floor (BSF), with a resistivity range from 0.1 to 2.5 Ωm, and this layer appears throughout the survey line. The second high-resistivity layer is approximately 190 to 300m BSF, with a resistivity range from 0.1 to 2.5 Ωm, and this layer appears throughout the survey line. The third high-resistivity layer is approximately 700m BSF, and it appears only near the RA receiver and has a higher resistivity than the other two layers.

According to our results, the locations of the first and second high-resistivity layers are less than 300m BSF. Because many reasons can cause abnormal resistivity, additional information is required. The third high-resistivity layer observed in Fig. 3a can be explained as follows: a) high-resistivity layers are present, but we do not have enough information to determine the reason, and b) the inversion algorithm may not converge well at these depths and may generate an unreasonably high resistivity.

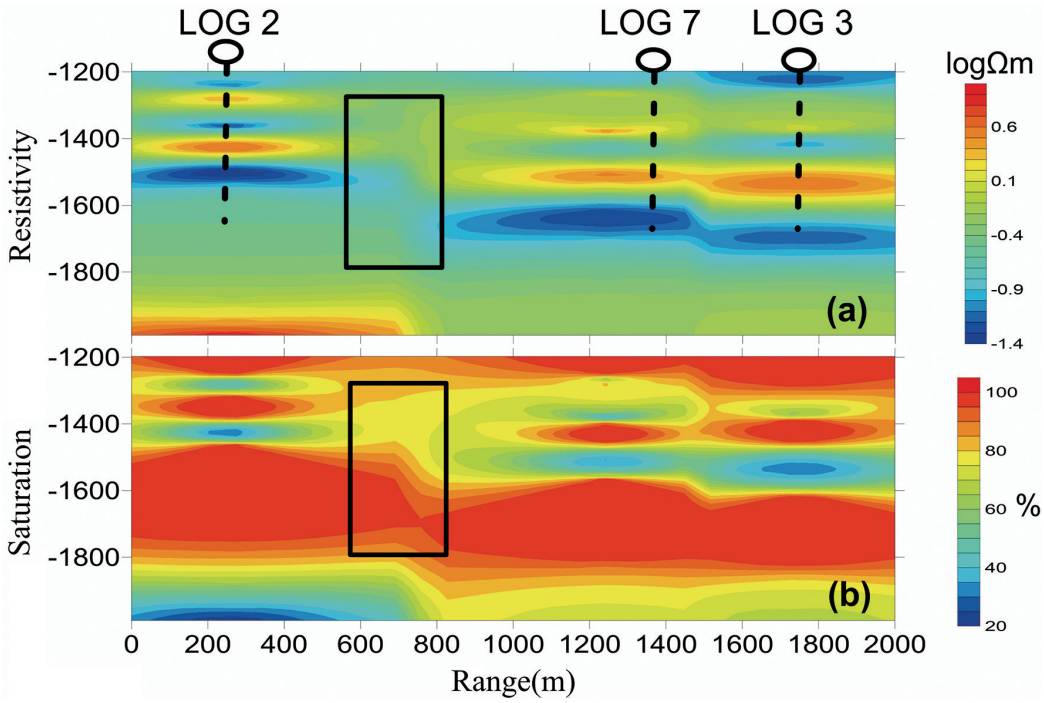

Fig. 3 - Resistivity results (a) and simplified saturation results (b).

Data from the log location are represented in Fig. 3a by the black lines. Highly anomalous resistivity values occur at depths of approximately 200-250m BSF beneath the survey line. The second instance of high conductivities below the resistive layer is observed at 270-300m BSF.

3. Discussion

Various active structures have been found in the study area in the Pearl River Mouth Basin, including faults, expulsion chimneys, and landslides. These three important findings are consistent with the geological literature and the seismic profile (Chen *et al.*, 2005; Wu *et al.*, 2011; Chiu *et al.*, 2014). During the formation of NGH, while enough free gas and some space is critical, expulsion chimneys provide a convenient path and allow the free gas to migrate directly (Zhang *et al.*, 2000; Sha *et al.*, 2005).

Because each different sounding method works on a different scale, improved constraints can likely be obtained by combining several different geophysical techniques in a single survey. The MCSEM method can provide considerably more insight during NGH exploration and characterisation when combined with seismic data and other data than when used as a single technique (Max, 1990). This supposition is supported by the high-amplitude reflection bands observed in the profiles, which indicate mild seismic activity at this site.

Considering other data such as seismic data, geology information, and log data that have been collected in this region, we mapped the gas structure in the conceptual model shown in Fig. 4 and highlighted the abnormal layers at the corresponding region. We selected only the portion in

which we were interested from the long profile. The electrical resistivity log, as a standard tool used to identify NGH, showed high resistivity in the blue region. Furthermore, the following seismic and EM data reflect anomalies in the same region.

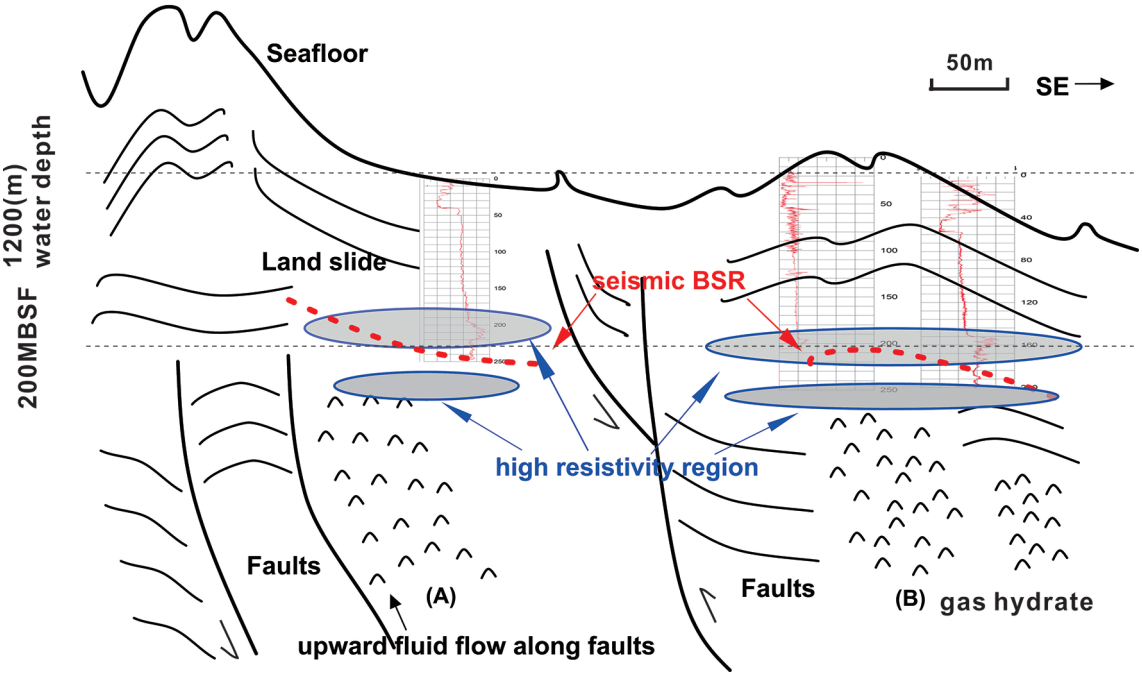

Fig. 4 - Conceptual model along a profile based on MCSEM, seismic, and log results.

The length is conceptual because the real ratio is unknown. The blue region represents the MCSEM results. The black lines are interpreted based on the seismic and geology information. The two interrupted BSR seismic lines indicate the existence of NGH at approximately 200m BSF along profile B (Figs. 3b and 4) (Wang *et al*., 2014). Expulsion chimneys provide a vertical path through which gas can migrate upwards. Fold and thrust faulting may result in approximate BSR structures that are parallel to the seabed in the area, which may in turn create a series of elongated thrust anticlines separated by deep synclines.

Based on the geophysical results in Fig. 4, we speculate that large volumes of NGH have accumulated, at least in the 200m BSF layer, thereby producing the observed anomalous resistivity. Some important geological variations were considered in our interpretation. For example, free gas is likely constrained by fault planes and expulsion chimneys (Chen *et al*., 2005; Liu *et al*., 2010; Wu *et al*., 2011). For long, deep expulsion chimneys, under the appropriate temperature and pressure, free gas may be transported to the seafloor based on the high resistivity in the seismic profile (Yin *et al*., 2008).

The first layer of the conceptual model may contain a reservoir of NGH that was able to migrate through cracks, fissures, or faults. Along the survey lines, NGH with high resistivity may have accumulated at depths between the seabed and the second layer. No additional information shows that massive carbonates exist at the third layer.

According to the conceptual model, the anomalous layers have low resolutions for the following reasons. First, the number of receiver sites is too small to control the profile. Second, the MCSEM results provide a more direct measure of the bulk hydrate concentration. Third, the experiment revealed a prominent resistivity anomaly, which was also indicated in the seismic reflection band along the transect. Finally, these results could be caused by gas hydrates and gas pockets, although sediment heterogeneities and carbonates may also play a role.

4. Conclusions

Approximately 40 km of the five MCSEM survey lines have been completed in the South China Sea in half a month. We use 1D inversion to obtain the resistivity distribution, and we obtain the saturation distribution by using Archie's law. Multifrequency joint inversion has been used in the interpretation.

The MCSEM data show three anomalous high-resistivity layers along the survey line in the SE direction. The log resistivity and the seismic data helped describe several hypothetical layered resistivity models. Then, we mapped the gas structure and positioned the abnormal layers at the corresponding points in the conceptual model.

According to the topography, the free gas migration paths and accumulation areas are interpreted and shown in the conceptual model. We suggest that there might be NGH in this survey area and mapped such an NGH distribution.

Future work will be completed, and 2D inversion will be used to obtain resistivity and depth values. Laboratory measurements should also be improved to characterise the electrical conductivity relationships of seafloor NGH at a higher resolution.

Acknowledgements. This research is supported by the Fundamental Research Funds for the Central Universities under Grant 53200859501, the National High Technology, Research and Development Program of China under Grant 2012AA09A201, and the Fundamental Research Funds of the Ministry of Education for the Central Universities under Grant GZH201100307. I would like to thank the "863" Program of the Institute of Marine Geology Survey Technology and the crew of the "Hai Yang Liu Hao" of Guangzhou Marine Geological Survey for their support during offshore operations.

REFERENCES

Archie G.E.; 1942: *The electrical resistivity log as an aid in determining some reservoir characteristics*. Trans. Am. Inst. Min. Metall. Eng., **146**, 54-61, doi: 10.2118/942054-g.

Behrens J.P.; 2005: *The detection of electrical anisotropy in 35 Ma Pacific lithosphere: results from a marine controlled-source electromagnetic survey and implications for hydration of the upper mantle*. Ph.D. Thesis in Earth Science, University of California, San Diego, CA, USA, 197 pp.

Boudou F., Le Stunff Y., Arnaud J., Esquier P., Kenworthy A., Whitfield P. and Soufleris C.; 2008: *Benefits of tilted transverse isotropy prestack depth migration for reservoir evaluation offshore West Africa*. First Break, **26**, 65-69, doi: 10.3997/1365-2397.2008009.

Chave A.D. and Thomson D.J.; 1987: *On the robust estimation of power spectra, coherences, and transfer functions*. J. Geophys. Res., **92**, 633-648, doi: 10.1029/jb092ib01p00633.

Chave A.D., Constable S.C. and Edwards R.N.; 1991: *Electrical exploration methods for the seafloor*. Electromagn. Methods Appl. Geophys., **2**, 931-966, doi: 10.1190/1.9781560802686.ch12.

Chen H., Wu X., Zhou D., Wang W. and Hao H.; 2005: *Meso-Cenozoic faults in Zhujiang River mouth basin and their geodynamic background*. J. Trop. Oceanogr., **24**, 52-61, doi: 10.3969/j.issn.1009-5470.2005.02.007, in Chinese with English abstract.

Chen H., Wang S., Chen Z., Yan W. and Li G.; 2014: *Geochemical and magnetic signals for the mud volcano-induced methane seepage in the core sediments of Shenhu area, northern South China Sea*. Environ. Earth Sci., **73**, 6365-6378, doi: 10.1007/s12665-014-3860-y.

Chen Q., Meng W., Wu M., Fan T., Zhang C., Qin X. and Li G.; 2015a: *A preliminary study on the present crustal stress of northern South China Sea*. Acta Geol. Sin., **89**, 320-321, doi: 10.1111/1755-6724.12423.

Chen K., Wei W., Deng M., Wu Z. and Yu G.; 2015b: *A new marine controlled-source electromagnetic receiver with an acoustic telemetry modem and arm-folding mechanism*. Geophys. Prospect., **63**, 1420-1429, doi: 10.1111/1365-2478.12297.

Chiu C.-S., Reeder B., Chiu L., Yang Y.J. and Chen C.; 2014: *South China Sea upper-slope sand dunes acoustics experiment*. J. Acoust. Soc. Am., **136**, 2316-2316, doi: 10.1121/1.4900394.

Coffin R., Hamdan L.J., Plummer R., Smith J., Gardner J. and Wood W.; 2008: *Analysis of methane and sulfate flux in methane charged sediments from the Mississippi Canyon, Gulf of Mexico*. Mar. Pet. Geol., **25**, 977-987, doi: 10.1016/j.marpetgeo.2008.01.014.

Collett T.S. and Ladd J.W.; 2000: *Detection of gas hydrate with downholelogs and assessment of gas hydrate concentrations (saturations) and gasvolumes on the Blake Ridge with electrical resistivity log data*. In: Paull C.K., Matsumoto R., Wallace P.J. and Dillon W.P. (eds), Proc. Ocean Drilling Program, Scientific Results, Texas A&M University, College Station, TX, USA, **164**, pp. 179-191, doi: 10.2973/odp.proc.sr.164.219.2000.

Constable S.; 2010: *Ten years of marine CSEM for hydrocarbon exploration*. Geophys., **75**, A67-A81, doi: 10.1190/1.3483451.

Constable S. and Srnka L.; 2007: *An introduction to marine controlled-source electromagnetic methods for hydrocarbon exploration*. Geophys., **72**, WA3-WA12, doi: 10.1190/1.2432483.

Evans R.L.; 2007: *Using CSEM techniques to map the shallow section of seafloor: From the coastline to the edges of the continental slope*. Geophys., **72**, WA105-WA116, doi: 10.1190/1.2434798.

Gallardo L.A. and Meju M.A.; 2004: *Joint two-dimensional DC resistivity and seismic travel time inversion with cross-gradients constraints*. J. Geophys. Res. - Solid Earth, **109**, B03311, doi: 10.1029/2003jb002716.

Goto T., Kasaya T., Takagi R., Sakurai N., Harada M., Sayanagi K. and Kinoshita M.; 2009: *Methane hydrate detection with marine electromagnetic surveys: case studies off Japan coast*. In: Proc. OCEANS 2009 Europe, Bremen, Germany, pp. 1-4.

Hsu S.-K., Chiang C.-W., Evans R.L., Chen C.-S., Chiu S.-D., Ma Y.-F., Chen S.-C., Tsai C.-H., Lin S.-S. and Wang Y.; 2014: *Marine controlled source electromagnetic method used for the gas hydrate investigation in the offshore area of SW Taiwan*. J. Asian Earth Sci., **92**, 224-232, doi: 10.1016/j.jseaes.2013.12.001.

Jegen M., Hoelz S., Swidinsky A., Sommer M., Berndt C. and Chi W.C.; 2014: *Electromagnetic and seismic investigation of methane hydrates offshore Taiwan - the Taiflux experiment*. In: Proc. OCEANS 2014, Taipei, Taiwan, pp. 1-4, doi: 10.1109/OCEANS-TAIPEI.2014.6964461.

Keller G.V.; 1966: *Electrical properties of rocks and minerals*. In: Clark S.P. Jr. (ed), Handbook of Physical Constant, Geological Society of America, Boulder, CO, USA, Memoirs 97, pp. 553-557.

Key K.; 2009: *1D inversion of multicomponent, multifrequency marine CSEM data: Methodology and synthetic studies for resolving thin resistive layers*. Geophys., **74**, F9-F20, doi: 10.1190/1.3058434.

Key K.; 2011: *Marine electromagnetic studies of seafloor resources and tectonics*. Surv. Geophys., **33**, 135-167, doi: 10.1007/s10712-011-9139-x.

Liu F., Tun S.-G. and Sun Y.-B.; 2010: *A quantitative analysis for submarine slope instability of the northern South China Sea due to gas hydrate dissociation*. Chin. J. Geophys., **53**, 946-953, doi: 10.3969/j.issn.0001-5733.2010.04.019.

Løseth H., Gading M. and Wensaas L.; 2009: *Hydrocarbon leakage interpreted on seismic data*. Mar. Petrol. Geol., **26**, 1304-1319, doi: 10.1016/j.marpetgeo.2008.09.008.

MacGregor L. and Sinha M.; 2000: *Use of marine controlled-source electromagnetic sounding for sub-basalt exploration*. Geophys. Prospect., **48**, 1091-1106, doi: 10.1046/j.1365-2478.2000.00227.x.

Max M.D.; 1990: *Gas hydrate and acoustically laminated sediments: potential environmental cause of anomalously low acoustic bottom loss in deep-ocean sediments*. Naval Research Lab., Washington, DC, USA, Final report, 72 pp.

Max M.D. (ed); 2003: *Natural gas hydrate in oceanic and permafrost environments*. Springer Science & Business Media, Dordrecht, the Netherlands, 415 pp.

Max M.D. and Johnson A.H.; 2014: *Hydrate petroleum system approach to natural gas hydrate exploration*. Petrol. Geosci., **20**, 187-199, doi: 10.1144/petgeo2012-049.

Max M.D., Johnson A.H. and Dillon W.P.; 2006: *Economic geology of natural gas hydrate*. Springer Science & Business Media, Dordrecht, the Netherlands, 342 pp.

Metcalfe G., Montagna F. and Tsinakis C.; 2014: *Amalgamation and interpolation in ordered algebras*. J. Algebra, **402**, 21-82, doi: 10.1016/j.jalgebra.2013.11.019.

Pearson C., Murphy J. and Hermes R.; 1986: *Acoustic and resistivity measurements on rock samples containing tetrahydrofuran hydrates: laboratory analogues to natural gas hydrate deposits*. J. Geophys. Res. - Solid Earth, **91**, 14132-14138, doi: 10.1029/JB091iB14p14132.

Qi Y., Huang L., Wu X., Fang G. and Yu G.; 2014: *Effect of loop geometry on TEM response over layered Earth*. Pure Appl. Geophys., **171**, 2407-2415, doi: 10.1007/s00024-014-0841-8.

Qi Y., Huang L., Wang X., Fang G. and Yu G.; 2017: *Airborne transient electromagnetic modeling and inversion under full attitude change*. IEEE Geosci. Remote Sens. Lett., **14**, 1575-1579, doi: 10.1109/lgrs.2017.2724558.

Sha Z., Wang H. and Zhang G.; 2005: *The relationships between diapir structure and gas hydrate mineralization*. Earth Sci. Front., **12**, 283-288, doi: US20090079972 A1.

Shao L., Li X., Wei G., Liu Y. and Fang D.; 2001: *Provenance of a prominent sediment drift on the northern South China Sea*. Sci. China Series D - Earth Sci., **44**, 919-925, doi: 10.1007/bf02907084.

Swidinsky A., Edwards R. and Jegen M.; 2013: *The marine controlled source electromagnetic response of a steel borehole casing: applications for the NEPTUNE Canada gas hydrate observatory*. Geophys. Prospect., **61**, 842-856, doi: 10.1111/1365-2478.12007.

Swidinsky A., Hölz S. and Jegen M.; 2015: *Rapid resistivity imaging for marine controlled-source electromagnetic surveys with two transmitter polarizations: an application to the North Alex mud volcano, west Nile Delta*. Geophys., **80**, E97-E110, doi: 10.1190/geo2014-0015.1.

Wang X., Li S. and Gong Y.; 2014: *Active tectonics and its effection on gas hydrates in northern South China Sea*. J. Jilin University - Earth Sci. Ed., **44**, 419-431, doi: 10.13278/j.cnki.jjuese.201402102.

Wang M., Deng M., Zhao Q., Luo X. and Jing J.; 2015: *Two types of marine controlled source electromagnetic transmitters*. Geophys. Prospect., **63**, 1403-1419, doi: 10.1111/1365-2478.12329.

Weitemeyer K.A.; 2008: *Marine electromagnetic methods for gas hydrate characterization*. Ph.D. in Earth Science, University of California, San Diego, CA, USA, 165 pp.

Weitemeyer K.A., Constable S., Key K. and Behrens J.; 2006: *First results from a marine controlled-source electromagnetic survey to detect gashydrates offshore Oregon*. Geophys. Res. Lett., **33**, L03304, doi: 10.1029/2005gl024896.

Weitemeyer K.A., Gao G., Constable S. and Alumbaugh D.; 2010: *The practical application of 2D inversion to marine controlled-source electromagnetic data*. Geophys., **75**, F199-F211, doi: 10.1190/1.3506004.

Winsauer W.O., Shearin H.M. Jr., Masson P.H. and Williams M.; 1952: *Resistivity of brine-saturated sands in relation to pore geometry*. Am. Ass. Pet. Geol. Bull., **36**, 253-277, doi: 10.1306/3D9343F4-16B1-11D7-8645000102C1865D.

Wu N., Zhang H., Yang S., Zhang G., Liang J., Lu J., Su X., Schultheiss P., Holland M. and Zhu Y.; 2011: *Gas hydrate system of Shenhu Area, northern South China Sea: geochemical results*. J. Geol. Res., **2011**, 1-10, doi: 10.1155/2011/370298.

Yin X., Zhou H., Yang Q., Wang H. and Chen J.; 2008: *The evidence for the existence of methane seepages in the northern South China Sea: abnormal high methane concentrations in bottom waters*. Acta Oceanol. Sin., **27(6)**, 62-70, doi: 10.1145/1360612.1360695.

Yin Z., Cai Z., Wan Z. and Lyu B.; 2015: *Features and dynamic mechanisms of Cenozoic tectonic migration and its impact on the hydrocarbon accumulation in the northern South China Sea*. Acta Oceanol. Sin., **34(1)**, 100-109, doi: 10.1007/s13131-015-0603-1.

Yu X., Wang J., Liang J., Li S., Zeng X. and Li W.; 2014: *Depositional characteristics and accumulation model of gas hydrates in northern South China Sea*. Mar. Pet. Geol., **56**, 74-86, doi: 10.1016/j.marpetgeo.2014.03.011.

Yuan J. and Edwards R.; 2000: *The assessment of marine gas hydrates through electrical remote sounding: hydrate without a BSR?* Geophys. Res. Lett., **27**, 2397-2400, doi: 10.1029/2000gl011585.

Zhang W., Li J., Zhong J., Fu Y., Chen S., Jiang L., Wang J. and Li M.; 2000: *A study on formation mechanism of gas chimney and relationship with petroleum*. Chin. J. Geol., **35**, 449-455.

Zhao Z., Sun Z., Wang Z., Sun Z., Liu J. and Zhang C.; 2015: *The high resolution sedimentary filling in Qiongdongnan Basin, northern South China Sea*. Mar. Geol., **361**, 11-24, doi: 10.1016/j.margeo.2015.01.002.

Corresponding author: Shengqing Xiong
China Aero Geophysical Survey & Remote Sensing Center for Natural Resources
Xueyuan Road 31, Haidian District, Beijing 100083, China
Phone: +86 18811518293; fax: +86 01082178779; e-mail: 23385165@qq.com